Available online at www.sciencedirect.com
SCIENCE DIRECT®
International Journal of Heat and Mass Transfer 48 (2005) 2652–2661
International Journal of HEAT and MASS TRANSFER
www.elsevier.com/locate/ijhmt

Laminar nanofluid flow in microheat-sinks

J. Koo, C. Kleinstreuer *

Department of Mechanical and Aerospace Engineering, North Carolina State University, Campus Box 7910, Raleigh, NC 27695-7910, USA

Received 20 December 2004; received in revised form 31 January 2005
Available online 2 April 2005

Abstract

In response to the ever increasing demand for smaller and lighter high-performance cooling devices, steady laminar liquid nanofluid flow in microchannels is simulated and analyzed. Considering two types of nanofluids, i.e., copper-oxide nanospheres at low volume concentrations in water or ethylene glycol, the conjugated heat transfer problem for microheat-sinks has been numerically solved. Employing new models for the effective thermal conductivity and dynamic viscosity of nanofluids, the impact of nanoparticle concentrations in these two mixture flows on the microchannel pressure gradients, temperature profiles and Nusselt numbers are computed, in light of aspect ratio, viscous dissipation, and enhanced temperature effects. Based on these results, the following can be recommended for microheat-sink performance improvements: Use of large high-Prandtl number carrier fluids, nanoparticles at high volume concentrations of about 4% with elevated thermal conductivities and dielectric constants very close to that of the carrier fluid, microchannels with high aspect ratios, and treated channel walls to avoid nanoparticle accumulation.

Keywords: Nanofluid; Brownian motion; Particle interaction; Effective thermal conductivity; Effective dynamic viscosity; Microheat-sink; Viscous dissipation

1. Introduction

In order to cope with ever increasing demands from the electronic, automotive and aerospace industries, cooling devices have to be small in size, light-weight and of high performance. The level and reliability of heat rejection efficiency largely determine the optimal design of cooling devices. Inspired by the microchannel heat-sink idea proposed by Tuckerman and Pease [1], several new designs and modeling approaches of high performance cooling devices have been proposed, including the fin model and the "porous medium" model. For example, Koh and Colony [2] introduced the porous medium model, which Tien and Kuo [3] expanded by adopting a modified Darcy's law for the momentum equation and volume-averaging for the energy equation. Kim et al. [4] compared analytically the one-equation and two-equation models for heat transfer in microchannel heat sinks. They reported that the one-equation model is valid only when the fluid phase is in local thermal equilibrium with the solid phase. They investigated parameters such as the Darcy number and conductivity ratio, which influence the validity of local thermal equilibrium, and concluded that the one-equation model is adequate for channels with high aspect ratios as well as for flows of highly conductive fluids. Zhao

* Corresponding author. Tel.: +1 919 5155261; fax: +1 919 5157968.
E-mail address: ck@eos.ncsu.edu (C. Kleinstreuer).

0017-9310/$ - see front matter © 2005 Elsevier Ltd. All rights reserved.
doi:10.1016/j.ijheatmasstransfer.2005.01.029

Nomenclature

A	Hamaker constant [J]
c	specific heat [J/kg K]
d	surface distance [m]
D	particle diameter [m]
f	modeling function [–]
k	thermal conductivity [W/m K]
n	refractivity [–]
n	particle number density [m^{-3}]
Nu	Nusselt number [–]
p	pressure [N/m^2]
Pr	the Prandtl number [–]
q	heat flux [W/m^2]
Re	Reynolds number [–]
T	temperature [K]
U_0	inlet velocity [m/s]
w	interparticle potential [J]
x	axial coordinate [m]
y	surface distance [m]
y,z	coordinates [m]

Greek symbols

α	volume fraction [–]
β	modeling parameter [–]
δ	boundary layer thickness [%]
κ	Boltzmann constant [J/K]
μ	dynamic viscosity [N s/m^2]
ρ	density [kg/m^3]
Φ	viscous dissipation function [s^{-2}]
θ	dimensionless temperature [–]

Superscripts/subscripts

m, n	exponents
c	continuous phase
d	discrete phase
f	fluid
l	liquid phase
m	mass flux mean value for liquid phase
*	dimensionless quantities
n	normal component
p	particle phase
s	solid (wall) phase
w	wall ($y = 0$)

and Lu [5] and Kim [6] compared the fin model and porous medium model. They suggested that the porous medium model is more accurate and more suitable for optimizing microchannels with high aspect ratios.

In order to further enhance microheat-sink performance, the use of nanofluids is proposed. Nanofluids, as coined by Choi [7], represent a new class of engineered heat transfer fluids which contain metallic or carbon-based particles with an average size of about 10 nm. Specifically, aluminum- and copper-oxide spheres as well as carbon-nanotubes of an average diameter of 30 nm were employed with volume concentrations of 0.001–6%. They generated, under static conditions, elevated thermal conductivities where $k_{\text{nanofluid}} < 3k_{\text{carrier fluid}}$ [8–10]. Thus, the use of nanofluids, for example in heat exchangers, may result in energy and cost savings and should facilitate the trend of device miniaturization.

Traditional theories, such as Maxwell [11] or Hamilton and Crosser [12], cannot explain this thermal phenomenon. Thus, new assessments and mathematical models of the new apparent (or effective) thermal conductivity have been proposed. For example, Xuan and Li [13] summarized previous experimental observations and concluded that $k_{\text{eff}} \equiv k_{\text{nanofluid}}$ was a function of both the thermal conductivities of the nanomaterial and carrier fluid, in terms of particle volume fraction, distribution, surface area, and shape. Yu and Choi [14,15] modified the Maxwell equation and Hamilton–Crosser relation for k_{eff} of solid-liquid suspensions to include the effect of ordered nanolayers around the particles. They also matched the model with observed conductivities by adjusting the nanolayer thickness and conductivity. Jang and Choi [16] suggested an effective thermal conductivity model considering the particles Brownian motion. They focused on the heat transfer between particles and carrier fluid, which is not directly related to the heat transfer phenomena in the fixed reference frame. Furthermore, the validity of their thermal boundary layer thickness, which they defined as $3\delta_{BF}/Pr$, where $Pr \sim \mathcal{O}(10)$ and δ_{BF} is the diameter of the fluid molecule, is questionable when applying the continuum approach together with their Nusselt number correlation. Kumar et al. [17] developed a new expression for the thermal conductivity, considering the increase of effective heat transfer area and particle motion. However, increasing the particle surface area is merely an indirect mechanism for heat transfer enhancement of the whole system. To consider the impact of particle Brownian motion, they replaced the particle-phase heat conductivity with $c \cdot \bar{u}_{\text{p}}$, which is problematic because the thermal conductivity is a property of the particle material. Koo and Kleinstreuer [18] developed a new, experimentally validated thermal conductivity model which takes the effects of particle Brownian motion and induced surrounding fluid motion into account (see Section 2.2).

While the previous thermal analyses focused on *quiescent* nanoparticle suspensions, Xuan and Li [19] studied heat transfer enhancement of water-based *Cu*-nanofluids in turbulent pipe flows. Wen and Ding [20] performed experiments with water-based Al_2O_3 nanofluids for laminar flow in a tube of 4.6 mm inside diameter and 6.4 mm outside tube diameter. While both of them reported improvements in heat transfer performances, they under-estimated the heat transfer performance by up to 40%, ignoring the important wall conduction effect for microchannels.

In this paper, considering nanofluid flow in a representative microchannel, conduction-convection heat transfer is analyzed for different base fluids, i.e., water and ethylene glycol with 20 nm CuO-nanoparticles, incorporating new k_{eff} and μ_{eff} models as well as the effect of viscous dissipation.

2. Theory

2.1. Basic transport equations

A typical multi-microchannel heat exchanger is depicted in Fig. 1, where the channel length is 1 cm with $a = 50$ μm, $H = 300$ μm, $t_0 = 25$ μm, and $W = 100$ μm. Focusing on the representative microchannel in the center, the coolant, i.e., liquid plus nanoparticles, flows in the x-direction and the heat flux from the source, q'', causes via conduction a wall heat flux, q_w, to the fluid. Assuming steady laminar flow of a dilute uniform suspension, and constant heat flux q'', the governing equations for this conjugated heat transfer problem can be written as follows.

Continuity:

$$\nabla \cdot \vec{u} = 0 \tag{1}$$

Momentum equation:

$$(\vec{u} \cdot \nabla)\vec{u} = -\frac{1}{\rho}\nabla p + \frac{\mu_{\text{eff}}}{\rho}\nabla^2 \vec{u} \tag{2}$$

Energy equation for fluid:

$$(\vec{u} \cdot \nabla)T = \frac{k_{\text{eff}}}{\rho c_{\text{p}}}\nabla^2 T + \frac{\mu_{\text{eff}}}{\rho c_{\text{p}}}\Phi \tag{3}$$

where

$$\Phi = \left(\frac{\partial u_i}{\partial x_j} + \frac{\partial u_j}{\partial x_i}\right)\frac{\partial u_i}{\partial x_j} \tag{4}$$

Energy equation for solid:

$$0 = \nabla^2 T \tag{5}$$

The associated boundary conditions are

$$u = U_0 \quad \text{at } x = 0 \tag{6}$$

$$\vec{u} = 0 \quad \text{at the wall} \tag{7}$$

$$\frac{\partial u}{\partial z} = 0 \quad \text{at } z = 0 \tag{8}$$

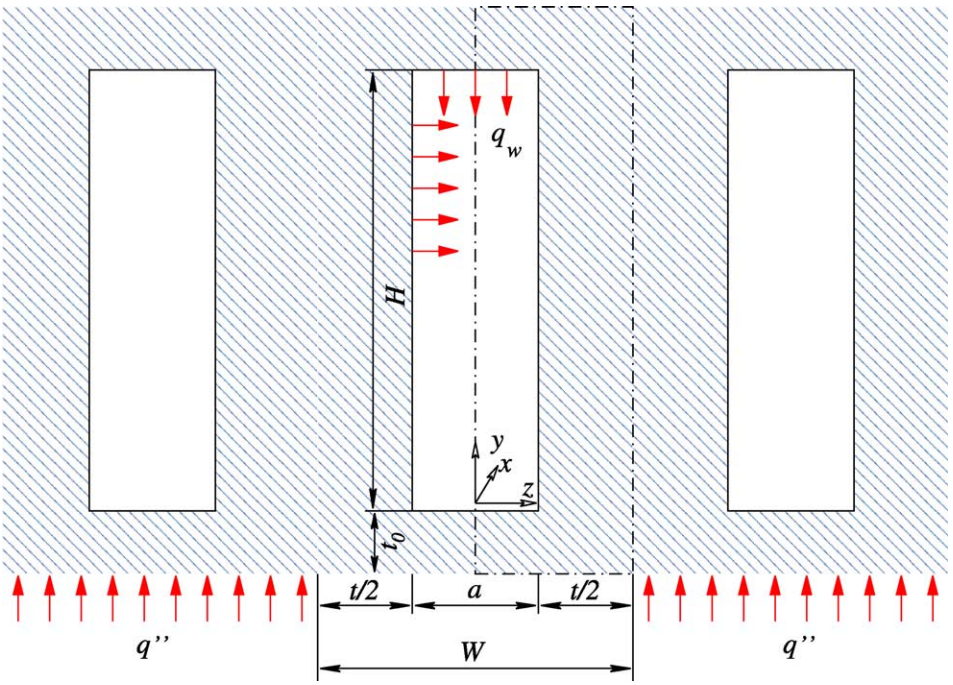

Fig. 1. Schematic of microheat-sink.

$$T_f = T_0 \quad \text{at } x = 0 \tag{9}$$

$$T_s = T_0 \quad \text{at } x = 0 \tag{10}$$

$$q'' = 0 \quad \text{at } x = 0, \quad x = L, \quad z = \frac{W}{2} \quad \text{and} \quad y = H + t_0 \tag{11}$$

$$k_s \frac{\partial T}{\partial y} = q'' \quad \text{at } y = -t_0 \tag{12}$$

$$k_s \nabla T_s|_n = k_{eff} \nabla T_f|_n \quad \text{at wall–fluid interfaces} \tag{13}$$

2.2. Effective thermal conductivity model

As alluded to in Section 1, the presence of nanoparticles at volume fractions $1 \leqslant \alpha_d \leqslant 4\%$ alter the mixture properties, i.e., $k_{liquid} \to k_{effective}$ and $\mu_{liquid} \to \mu_{effective}$. While μ_{liquid} does not differ measurably from μ_{eff} for $Pr > 1$, major heat transfer improvements center around k_{eff} for which a new model has been proposed. Specifically, the k_{eff}-model for nanofluids considers the impact of particle Brownian motion and that of the particle interaction potential [18]. The new model is composed of two parts, the conventional static part as well as a dynamic part which originates from the particle Brownian motion.

$$k_{eff} = k_{static} + k_{Brownian} \tag{14}$$

where, for example, according to Maxwell [11]

$$\frac{k_{static}}{k_c} = 1 + \frac{3\left(\frac{k_d}{k_c} - 1\right)\alpha_d}{\left(\frac{k_d}{k_c} + 2\right) - \left(\frac{k_d}{k_c} - 1\right)\alpha_d} \tag{15}$$

Here, α_d is the particle volume fraction, k_c is the thermal conductivity of the carrier fluid, and k_d is that of the particles.

The $k_{Brownian}$ term was developed using kinetic theory together with Stokes' flow approximation to estimate the size of the affected fluid-parcel moving with each particle.

$$k_{Brownian} = 5 \times 10^4 \beta \alpha_d \rho_l c_l \sqrt{\frac{\kappa T}{\rho_d D}} f(T, \alpha_d, \text{ etc.}) \tag{16}$$

The two modeling functions β and f were introduced to consider the hydrodynamic interaction among the Brownian motion induced (moving) fluid parcels, and the particle interaction due to the particle interaction potential to encapsulate the strong temperature dependence, respectively. Specifically, the function f depends on properties of the intervening fluid, and hence particle interactions. Traditionally, the interparticle potential, $w(d)$, can be used to take that into consideration, i.e.,

$$w(d) = -\frac{AR}{6d} \tag{17}$$

where A is the Hamaker constant, R is the particle radius, and d is the surface distance. The Hamaker constant A for two identical phases 1 interacting across medium 3 can be expressed as [21]:

$$A \approx \frac{3}{4} \kappa T \left(\frac{\epsilon_1 - \epsilon_3}{\epsilon_1 + \epsilon_3}\right)^2 \tag{18}$$

where ϵ is the electric dipole constant. Based on experimental evidence, for water-based CuO-nanofluids, β and f were estimated as [18]:

$$\beta = 0.0137(100\alpha_d)^{-0.8229} \quad \text{for } \alpha_d < 1\% \tag{19a}$$

$$\beta = 0.0011(100\alpha_d)^{-0.7272} \quad \alpha_d > 1\% \tag{19b}$$

and

$$f(T, \alpha_d) = (-6.04\alpha_d + 0.4705)T + (1722.3\alpha_d - 134.63) \quad 1 < \alpha_d < 4\% \quad 300 < T < 325 \text{ K} \tag{20}$$

It should be noted that the function f is a linear equation because of the Taylor series truncation; but, that functional dependence can be confirmed with Eqs. (17) and (18) as well. It is observed that β is quite independent of the particle type for low concentration cases (say, $\alpha_d < 1\%$), while it exhibits a strong particle material dependence for relatively high concentration cases (say, $\alpha_d > 1\%$).

Employing the same concept for the derivation of the effective viscosity due to Brownian motion, it can be stated that:

$$\mu_{eff} = \mu_{static} + \mu_{Brownian} \tag{21}$$

where

$$\mu_{Brownian} = \frac{k_{Brownian}}{k_l} \times \frac{\mu_l}{Pr_l} \tag{22}$$

Thus, the effect of Brownian motion on the effective fluid viscosity is less significant than that on the effective thermal conductivity, since $Pr_l > 1$ for liquids. At room temperature, the Prandtl number is about 5, 100, and 5000 for water, ethylene glycol, and engine oil, respectively, while for $T \equiv 350$ K, the values are 2.3, 34.6, and 546.

Krieger [22] stated that the common structural feature unifying rheologically interesting class of fluids is the presence of constituents, either colloidal particles or macromolecules, whose dimensions are large compared with molecules of the suspending medium, while still small enough to exhibit significant rotatory and translatory Brownian movement. The structure of the fluid resembles a gas of large molecules, with the void space replaced by a Newtonian continuum. The newly developed effective thermal conductivity and dynamic viscosity models well comply with his statement by applying the kinetic theory for the gas-like behavior and considering the induced liquid motion considering the Newtonian continuum replacing the void space.

3. Results and discussion

The thermal nanofluid flow results, focus on four aspects: hydrodynamics, temperature gradients, Nusselt numbers, and wall effects. It should be noted that the results for ethylene glycol based nanofluids do not contain the impact of the function f due to the lack of experimental data. Therefore, comparisons between ethylene glycol- and water-based nanofluids are performed by setting $f = 1$ (Table 1).

3.1. Nanofluid flows

Setting $f \equiv 1$ for both test fluids, so that any additional temperature influence is ignored, Fig. 2 summarizes the impact of nanofluids with different particle concentrations on the effective thermal conductivity, $\hat{k}_{\text{eff}|_{x=8\ \text{mm}}} = k_{\text{eff}}/k_{\text{l}}$, and the necessary pressure gradient, $\hat{p} = (p_{\text{in}} - p_{exit})/(p_{\text{in},\alpha_{\text{d}}=0} - p_{\text{exit},\alpha_{\text{d}}=0})$, to maintain the mixture flow rate.

Although the changes in $\hat{p}$ are slightly higher for ethylene glycol-based nanofluids, the thermal conductivity increases significantly due to the higher Prandtl number. This was confirmed by Lee et al. [23], Xie et al. [24,25] who reported that ethylene glycol-based nanofluids showed a larger increase in thermal conductivity than water-based ones. Indeed, by comparing $k_{\text{Brownian}}/k_{\text{static}} \sim \rho_{\text{l}} c_{\text{l}}/k_{\text{l}}$, which is the ratio of dynamic part and static part of the effective thermal conductivity (see Eq. (16)), Koo and Kleinstreuer [18] showed that this is a result of Brownian motion of the nanoparticles.

Table 1
Experimental data; d: particle diameter, α: volume fraction

Author(s)	Material	Liquid	d (nm)	α (%)	Findings
Lee et al. [23]	Al_2O_3/CuO	Water, ethylene glycol	38.4/23.6	1–5	Al_2O_3 good agreement with H–C model/ CuO: showed higher conductivity than H–C model predicts. Ethylene glycol-based nanofluids showed higher value. Al_2O_3 suspensions showed higher value
Masuda et al. [31]	Al_2O_3	Water	13	4.3	Showed higher conductivity than H–C model predicts. Considered non-spherical particles
Pak and Cho [29]	Al_2O_3, TiO_2	Water	13/27	1–4.5	Both suspensions showed higher effective thermal conductivity than conventional theory predicts. Al_2O_3 suspension showed higher effective thermal conductivity. Effective viscosity increased maximum 200%
Xuan and Li [13]	Cu	Water	100	0.3–2	The suspension showed higher effective thermal conductivity than Maxwell relation predicts
Eastman et al. [9]	Cu, Al_2O_3, CuO	Water, ethylene glycol	<10	0.3	Anomalously increased effective thermal conductivity (40%)
Choi [8]	Nanotubes	α-Olefin oil	$\sim 25 \times 50 \times 10^3$	0–1	Anomalously increased effective thermal conductivity (160%)
Xie et al. [24]	Al_2O_3	Ethylene glycol, water, pump oil	12–302	0–5	All suspensions showed higher value than H–C model predicts. $k_{\text{eff,DW}} < k_{\text{eff,EG}} < k_{\text{eff,DE}}$. They observed that pH value and specific surface area of nanoparticles affected the effective thermal conductivity
Das et al. [30]	Al_2O_3/CuO	Water	38.4/28.6	1–4	Both suspensions showed higher value than Maxwell relation predicts. Al_2O_3 suspension showed higher value. They observed temperature dependence of the effective thermal conductivity
Patel et al. [10]	Au-citrate/ Ag-citrate	Water, toluene	15/70	0.00013–0.011	Both suspensions showed higher value than Maxwell relation predicts. Both suspensions showed measurable increase even with very small concentrations. They observed temperature dependence
Xie et al. [25]	Nanotubes	Distilled water, ethylene glycol, decene	$15 \times 30 \times 10^3$	0.1–1.0	All suspensions showed higher value than H–C model predicts. $k_{\text{eff,DW}} < k_{\text{eff,EG}} < k_{\text{eff,DE}}$

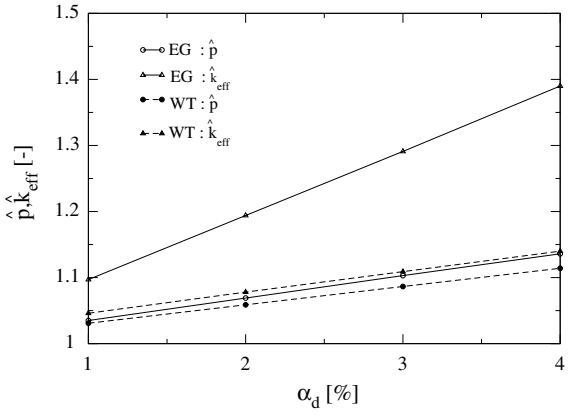

Fig. 2. Comparisons of volume fraction dependent pressure gradients, $\hat{p} \equiv (p_{in} - p_{exit})/(p_{in,\alpha_d=0} - p_{exit,\alpha_d=0})$ and effective thermal conductivities at $x = 8$ mm for ethylene glycol (EG)- and water (WT)-based CuO-nanofluids (temperature function $f \equiv 1$).

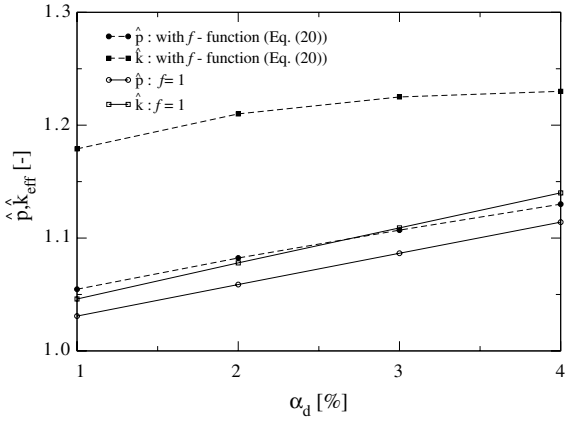

Fig. 3. Influence of temperature-function f on dimensionless pressure gradient and effective thermal conductivity for water-based CuO nanofluids.

Due to the lack of published experimental data to estimate the function f for different carrier fluids, its influence could only be analyzed for water-based CuO-nanofluids (c.f. Eq. (20)). Fig. 3 shows the effect of f on the driving force and the effective thermal conductivity. Clearly, the improvement in heat transfer performance outweighs the inherent cost of higher $\hat{p}$-values. Future work will consider the impact of f on enhanced heat transfer performance of ethylene glycol-based nanofluids as well.

3.2. Temperature profiles

In this section, the effects of nanofluids and viscous dissipation on temperature profiles are discussed in terms of non-dimensional temperatures.

Solid phase:

$$\theta_s = \frac{\overline{T}_s - \overline{T}_w}{\frac{\bar{q}_w H}{(1-\epsilon)k_s}} \tag{23}$$

Fluid phase:

$$\theta_f = \frac{\overline{T}_f - \overline{T}_w}{\frac{\bar{q}_w H}{(1-\epsilon)k_s}} \tag{24}$$

where all variables are locally averaged. T_w is the heat-capacity-averaged temperature at $y = 0$.

3.2.1. Effects of base fluid and viscous dissipation

Figs. 4 and 5 compare the dimensionless temperature variations across the microchannel, $0 \leqslant y \leqslant H$, for ethylene glycol- and water-based nanofluids. The temperature difference between the solid and liquid phases is greater for ethylene glycol due to its lower thermal conductivity. The solid-phase temperature profiles are not affected by viscous dissipation. That effect is more

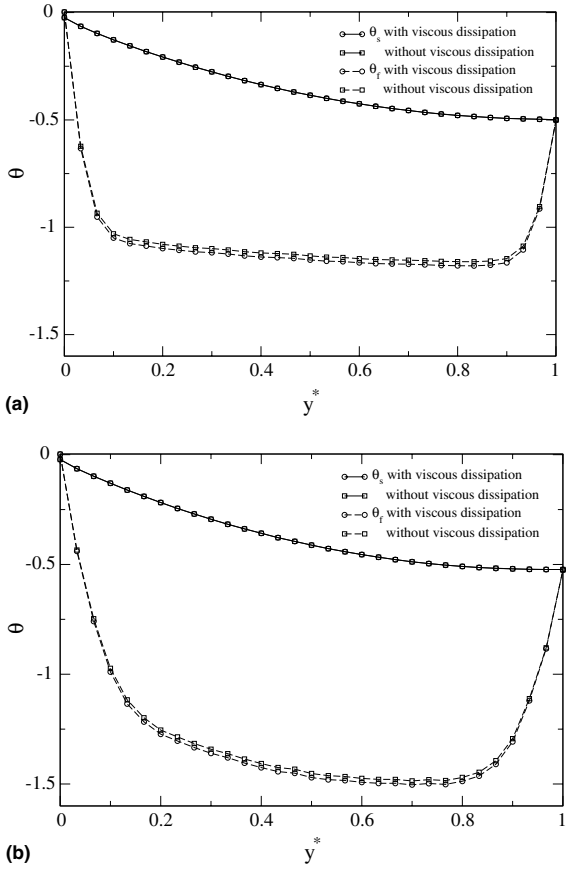

Fig. 4. The viscous dissipation effect on non-dimensional temperature profiles for ethylene glycol-based CuO nanofluids ($\alpha_d = 4\%$, $y^* = y/H$, $f \equiv 1$); (a) $x = 0.0006$ m, and (b) $x = 0.008$ m.

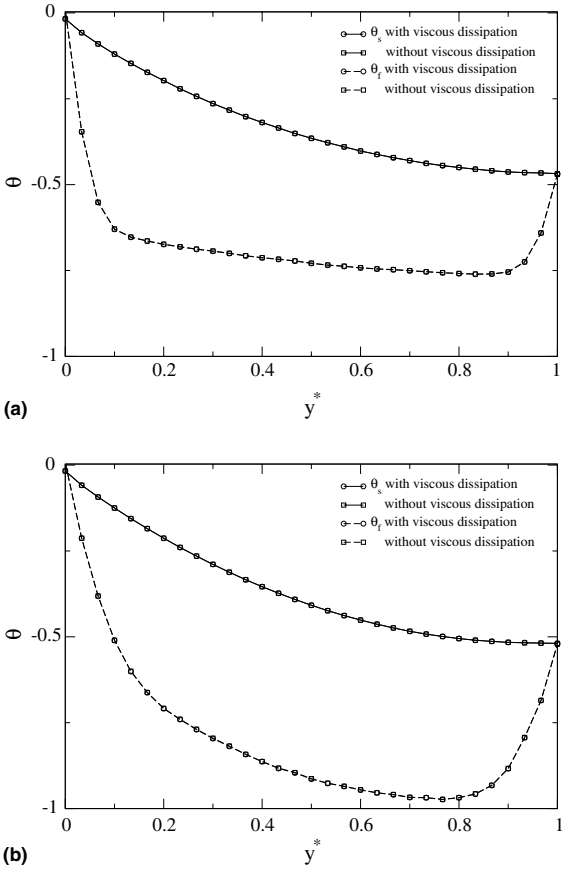

Fig. 5. The viscous dissipation effect on non-dimensional temperature profiles for water-based CuO nanofluids (α_d = 4%, $f \equiv 1$); (a) x = 0.0006 m, and (b) x = 0.008 m.

pronounced for ethylene glycol(EG)-based nanofluids due to its higher dynamic viscosity and lower heat capacity compared to water-based ones. For EG-based nanofluids, the fluid temperature profiles without the viscous dissipation term are always higher, which potentially incorrectly leads to higher Nusselt numbers.

Reducing the channel width by half (now a = 25 μm), the resulting influence on the temperature profile of the EG-nanofluid is given in Fig. 6. The inlet velocity was kept at 2.2 m/s, because the total mass flow rate in the system is the same due to the increase of the number of channels.

3.2.2. Comparison of cooling performance between pure fluid and nanofluid

In order to assess the impact of the channel inlet velocity on solid- and fluid-phase temperature profiles of pure ethylene glycol and EG-based nanofluids (Fig. 7(a)), the pressure drop requirement was kept the same for the cases U_0 = 2.2 m/s and U_0 = 2.5 m/s as well as α_d = 0% and 4%. While the impact of ΔU_0 = 0.3 m/s is

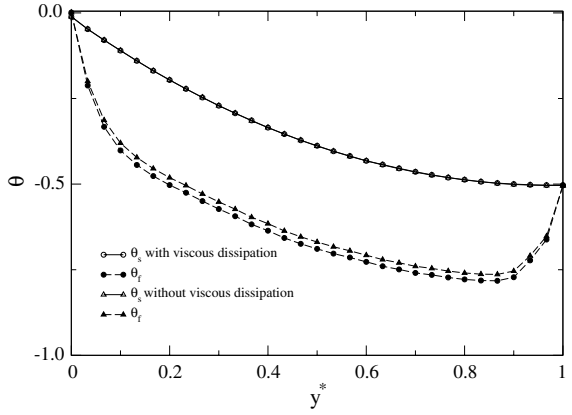

Fig. 6. The effect of viscous dissipation term of EG nanofluid (α_d = 4%) on the heat transfer performance in a channel of width (a = 25 μm, $f \equiv 1$).

negligible, the influence of the presence of CuO-particles is significant.

3.2.3. Impact of the f-function

Turning again to water-based nanofluids, the influence of the augmenting temperature-function f (see Eq. (20)) can be evaluated. As shown in Fig. 7(b), the f-function improves heat transfer performance. However, the temperature difference is less for the cases considering the f-function compared to those without it, because the slope of the f-function decreases with particle concentration for the given carrier fluid of the mixture.

3.3. The Nusselt number

3.3.1. Base fluid effect

Nusselt number comparisons for the two nanofluids are shown in Fig. 8. The Nusselt numbers ($Nu = \frac{hD_h}{k_{eff}}$) were calculated at stations x = 0.0006, 0.005, and 0.008 m. The heat transfer coefficient h was calculated as

$$h = \frac{\bar{q}_w}{\overline{T}_w - T_m} \tag{25}$$

where $\bar{q}_w = q'' \frac{W}{2\cdot(H+a)}$ and q'' is the heat flux from the bottom plate, $\overline{T}_w$ is the averaged wall temperature, and T_m is the mass-flux-averaged fluid temperature. The effect of axial conduction heat transfer along the wall was found to be negligible for the given configuration. The Nusselt numbers for EG-based nanofluids are always higher than for the water-based ones. This is due to the fact that EG-based nanofluids are experiencing stronger thermal flow development effects.

For a given location, the Nusselt number decreases with the volume fraction α_d, where the effect is more profound for EG-based nanofluids. This is attributed mainly to both different increase rates of the effective

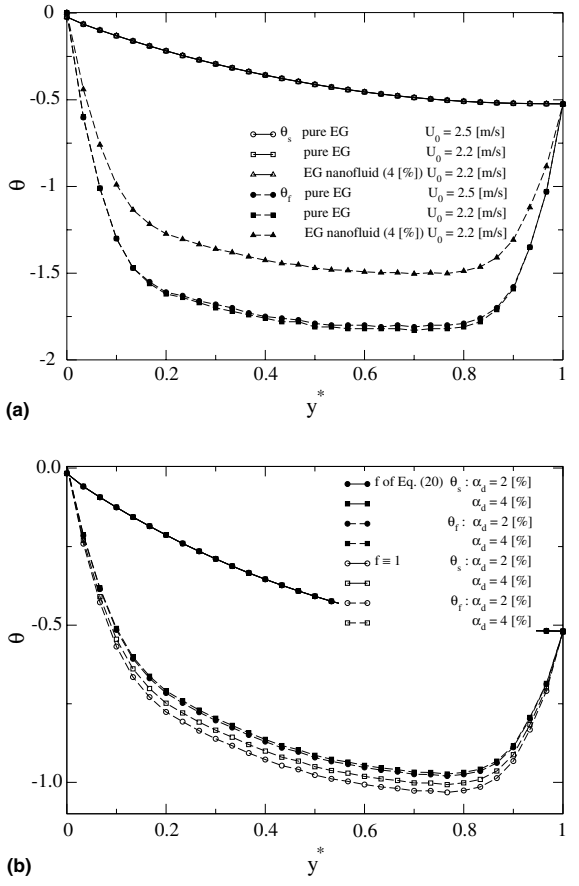

Fig. 7. (a) Comparison of temperature profiles of pure-fluid cooling and nanofluid cooling cases ($f \equiv 1$); (b) The effect of function f on temperature profiles.

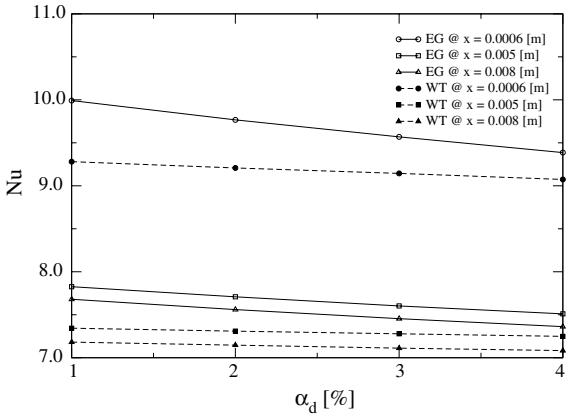

Fig. 8. Nusselt number comparisons for ethylene glycol- and water-based nanofluids with different CuO-volume fractions ($q'' = 100$ W/cm^2, $f \equiv 1$).

thermal conductivity k_{eff} and the heat transfer coefficient h, and the heat generation due to viscous dissipation. The effective thermal conductivity and dynamic viscosity increase is proportional to the particle concentration α_d. The heat transfer coefficient h is roughly proportional to $Re^m \cdot Pr^n$, where m and n are 1/3 for laminar flows, so it is proportional to $\alpha_d^{-1/3}$. Therefore, the Nusselt number decreases proportional to $\frac{Pr^{1/3}}{\alpha_d^{1/3}}$. The Nusselt number of ethylene glycol-based nanofluids decreases more with particle concentration α_d due to the higher Prandtl numbers.

3.3.2. Viscous dissipation effect

As indicated in Fig. 8, the Nusselt numbers are higher by 2.2% for the base configuration ($a = 50$ μm). Although this is not a significant increase, it implies that the viscous dissipation effect affects the thermal performance of ethylene glycol-based nanofluids, which is not the case for water-based ones. It is observed that the Nusselt number is 12.93 with viscous dissipation and 13.93 without it for flow in channels of half width (see Fig. 4). The difference is 7.7% which is about 3.5 times that for the base case. Clearly, the viscous dissipation effect becomes more important for flows in very narrow channels. Thus, the heat transfer performance cannot be endlessly improved by simply adopting narrow channels. The increase in Nusselt number is due to the higher aspect ratios.

3.3.3. Influence of the f-function

The non-dimensional fluid temperature is higher for the cases considering the influence of the function f as shown in Fig. 7(b), which implies that the actual temperature dependence of nanofluids improves heat transfer performance. However, the Nusselt number decreases slightly when considering the f-function (Fig. 9). This is due to the fact that the effective thermal conductivity

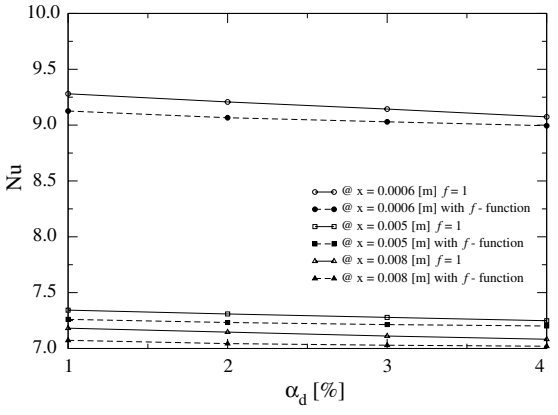

Fig. 9. The effect of function f on the Nusselt number.

increases at a higher rate than the heat transfer coefficient does ($\Delta h \sim \Delta Re^{1/3} \sim \Delta \nabla_x p^{1/3}$, see Fig. 3).

3.4. Particle–particle and particle–wall interactions

As discussed by Koo and Kleinstreuer [18], the particle interaction plays an important role in high concentration suspensions. Without the help of either electrostatic stabilization or steric stabilization, particles will flocculate or coagulate when they are brought together via Brownian motion. For example, most metal oxides have a surface layer of the metal hydroxide which is amphoteric in nature and can become either positively or negatively charged, depending on the pH to generate the electrical double layer [26]. Particles will flocculate when the energy of the electrostatic barrier is not greater than the particle kinetic energy, such that the particle can overcome the energy barrier [27]. In reality, the speed of particles shows a Maxwellian distribution [28], and there always exists a fraction of particles which have enough kinetic energy to overcome the energy barrier resulting in flocculation. That possible increase in average particle size might diminish the benefits of nanofluids.

Interactions between wall and particle could be even more problematic. In a quiescent environment, such as in an experimental apparatus to measure the effective thermal conductivity of nanofluids, the wall effect might be not so significant if the size of the vessel is large. However, the particle–liquid–wall interactions become important for flows in microchannels where the surface area of the wall is relatively large. Assuming a much smaller impact region of the double-layer than that of particle attraction, and no flocculation, the equilibrium nanoparticle distribution was derived considering the particle–liquid–wall attraction ($= \frac{AD}{12y^2}$ [21]) and the thermal Brownian forces ($= \kappa T \nabla \ln n$ [27]) as

$$n(y) = C \exp\left(-\frac{A}{12\kappa T}\frac{D}{y}\right) \tag{26}$$

where y is the distance from the wall. The nanoparticle distribution depends on the particle size D, and the Hamaker constant A (see Eq. (18)) which is a function of the material properties of the particle, wall, and carrier fluid. Fig. 10 shows the effect of particle–liquid–wall interactions on the nanoparticle distribution near the wall for different nanofluids, where n_0 is the centerline number density. When particles and the wall attract each other, i.e., $A > 0$, the concentration near the wall increases as it approaches the wall. In contrast, it decreases when particles and the wall repulse each other, i.e., $A < 0$. The concentration can change near the wall up to 18% due to the interaction. If the wall material is such that there exists a strong attractive force between particle and wall surface, particles would deposit on the wall forming a layer. In turn, particles would deposit on the mono-layer due to the strong attraction between the particle layer and approaching particles.

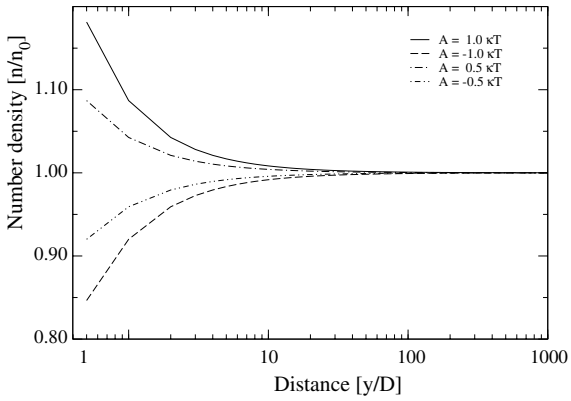

Fig. 10. The particle–liquid–wall interaction effect on nanoparticle distribution near the wall.

The newly developed thermal conductivity and dynamic viscosity model indicates ways to avoid this problem. The strength of the attraction is proportional to the Hamaker constant (see Eq. (18)). Therefore, the problem could be resolved by selecting appropriate particle-fluid and particle-solid pairs to minimize the Hamaker constant.

4. Conclusions

It has been shown that the addition of nanoparticles, e.g., CuO-particles of mean diameter $D = 20$ nm at low volume fractions $1 \leqslant \alpha_d \leqslant 4\%$, to high-Prandtl number liquids significantly increases the heat transfer performance of microheat-sinks. As a result of the present analysis for a representative microchannel, the following recommendations are made to maximize the merits of adding nanoparticles.

- A base fluid of high-Prandtl number, e.g., ethylene glycol and oils, should be used.
- Nanoparticles of high thermal conductivity are advantageous.
- A channel with high aspect ratio is desirable.

In order to minimize particle–particle and particle–wall interaction problems, it is suggested to:

- Select particles with a dielectric constant which is very close to that of the base fluid;
- Select a wall material such that particle–wall attraction is minimized;
- Treat the wall and particles to increase the energy barrier among them.

Acknowledgement

The authors want to express thanks to Dr. Joseph P. Archie and Sarah Archie for the endowment the McDonald-Kleinstreuer fellowship for Junemo Koo.

References

[1] D. Tuckerman, R. Pease, High-Performance heat sinking for VLSI, IEEE Electron Dev. Lett. EDL-2 (5) (1981) 126–129.
[2] J. Koh, R. Colony, Heat transfer of microstructures for integrated circuits, Int. Commun. Heat Mass Transfer 13 (1986) 89–98.
[3] C.L. Tien, S.M. Kuo, Analysis of forced convection in microstructures for electronic system cooling, in: Proc. Int. Symp. Cooling Technology for Electronic Equipment, Honolulu, HI, 1987, pp. 217–226.
[4] S.J. Kim, D. Kim, D. Lee, On the local thermal equilibrium in microchannel heat sinks, Int. J. Heat Mass Transfer 43 (2000) 1735–1748.
[5] C.Y. Zhao, T.J. Lu, Analysis of microchannel heat sinks for electronics cooling, Int. J. Heat Mass Transfer 45 (2002) 4857–4869.
[6] S. Kim, Methods for thermal optimization of microchannel heat sinks, Heat Transfer Eng. 25 (2004) 37–49.
[7] S. Choi, Enhancing thermal conductivity of fluids with nanoparticles, FED 231 (1995) 99–103.
[8] S. Choi, Z. Zhang, W. Yu, F. Lockwood, E. Grulke, Anomalously thermal conductivity enhancement in nanotube suspensions, Appl. Phys. Lett. 79 (14) (2001) 2252–2254.
[9] J. Eastman, S. Choi, S. Li, W. Yu, L. Thompson, Anomalously increased effective thermal conductivities of ethylene glycol-based nanofluids containing copper nanoparticles, Appl. Phys. Lett. 78 (2001) 718–720.
[10] H. Patel, S. Das, T. Sundararajan, A. Sreekumaran, B. George, T. Pradeep, Thermal conductivities of naked and monolayer protected metal nanoparticle based nanofluids: Manifestation of anomalous enhancement and chemical effects, Appl. Phys. Lett. 83 (14) (2003) 2931–2933.
[11] J. Maxwell, A Treatise on Electricity and Magnetism, second ed., Oxford University Press, Cambridge, UK, 1904.
[12] R. Hamilton, O. Crosser, Thermal conductivity of heterogeneous two-component systems, I&EC Fundam. 125 (3) (1962) 187–191.
[13] Y. Xuan, Q. Li, Heat transfer enhancement of nanofluids, Int. J. Heat Fluid Flow 21 (2000) 58–64.
[14] W. Yu, S. Choi, The role of interfacial layers in the enhanced thermal conductivity of nanofluids: A renovated Maxwell model, J. Nonoparticle Res. 5 (2003) 167–171.
[15] W. Yu, S.U.S. Choi, The role of interfacial layers in the enhanced thermal conductivity of nanofluids: A renovated Hamilton-Crosser model, J. Nanoparticle Res. 6 (4) (2004) 355–361.
[16] S.P. Jang, S.U.S. Choi, Role of Brownian motion in the enhanced thermal conductivity of nanofluids, Appl. Phys. Lett. 84 (21) (2004) 4316–4318.
[17] D.H. Kumar, H.E. Patel, V.R.R. Kumar, T. Sundararajan, T. Pradeep, S.K. Das, Model for heat conduction in nanofluids, Phys. Rev. Lett. 93 (14) (2004).
[18] J. Koo, C. Kleinstreuer, A new thermal conductivity model for nanofluids, J. Nanoparticle Res. 6 (2004), in press.
[19] Y. Xuan, Q. Li, Investigation on convective heat transfer and flow features of nanofluids, J. Heat Transfer 125 (2003) 151–155.
[20] D. Wen, Y. Ding, Experimental investigation into convective heat transfer of nanofluids at the entrance region under laminar flow conditions, Int. J. Heat Mass Transfer 47 (2004) 5181–5188.
[21] J. Israelachvili, Intermolecular and Surface Forces, second ed., Academic Press, Amsterdam, 1992.
[22] I.M. Krieger, Rheology of monodisperse lattices, Adv. Colloid Interf. Sci. 3 (1972) 111–136.
[23] S. Lee, S. Choi, S. Li, J. Eastman, Measuring thermal conductivity of fluids containing oxide nanoparticles, J. Heat Transfer 121 (1999) 280–289.
[24] H. Xie, T. Wang, J. Xi, Y. Liu, F. Ai, Q. Wu, Thermal conductivity enhancement of suspensions containing nanosized alumina particles, J. Appl. Phys. 91 (7) (2002) 4568–4572.
[25] H. Xie, H. Lee, W. Youn, M. Choi, Nanofluids containing multiwalled carbon nanotubes and their enhanced thermal conductivities, J. Appl. Phys. 94 (8) (2003) 4967–4971.
[26] R.J. Hunter, Introduction to Modern Colloid Science, Oxford Science Publications, Oxford, UK, 2003.
[27] R. Probstein, Physicochemical Hydrodynamics, second ed., Wiley Interscience, Hoboken, NJ, 2003.
[28] D. Schroeder, An Introduction to Thermal Physics, Addison Wesley Longman, San Francisco, CA, 2000.
[29] B. Pak, Y. Cho, Hydrodynamic and heat transfer study of dispersed fluids with submicron metallic oxide particles, Exp. Heat Transfer 11 (1998) 151–170.
[30] S. Das, N. Putra, P. Thiesen, W. Roetzel, Temperature dependence of thermal conductivity enhacement for nanofluids, J. Heat Transfer 125 (2003) 567–574.
[31] H. Masuda, A. Ebata, K. Teramae, N. Hishinuma, Alteration of thermal conductivity and viscosity of liquid by dispersion ultra-fine particles, Netsu Bussei (Japan) 4 (43) (1993) 227–233.